THE ASTROPHYSICAL JOURNAL, 482:782–791, 1997 June 20


# RATES FOR PARALLAX-SHIFTED MICROLENSING EVENTS FROM GROUND-BASED OBSERVATIONS OF THE GALACTIC BULGE

ARI BUCHALTER
Department of Astronomy, Columbia University, Box 46, Pupin Hall, 538 West 120th Street, New York, NY 10027;
ari@parsifal.phys.columbia.edu

AND

MARC KAMIONKOWSKI
Department of Physics, Columbia University, 538 West 120th Street, New York, NY 10027; kamion@phys.columbia.edu
*Received 1996 April 24; accepted 1997 January 15*

## ABSTRACT

The parallax effect in ground-based microlensing (ML) observations consists of a distortion to the standard ML light curve arising from the Earth's orbital motion. This can be used to partially remove the degeneracy among the system parameters in the event timescale, $t_0$. In most cases, the resolution in current ML surveys is not accurate enough to observe this effect, but parallax could conceivably be detected with frequent follow-up observations of ML events in progress, providing the photometric errors are small enough. We calculate the expected fraction of ML events where the shape distortions will be observable by such follow-up observations, adopting Galactic models for the lens and source distributions that are consistent with observed microlensing timescale distributions. We study the dependence of the rates for parallax-shifted events on the frequency of follow-up observations and on the precision of the photometry. For example, we find that for hourly observations with typical photometric errors of 0.01 mag, 6% of events where the lens is in the bulge, and 31% of events where the lens is in the disk (or $\approx 10\%$ of events overall), will give rise to a measurable parallax shift at the 95% confidence level. These fractions may be increased by improved photometric accuracy and increased sampling frequency. While long-duration events are favored, the surveys would be effective in picking out such distortions in events with timescales as low as $t_0 \approx 20$ days. We study the dependence of these fractions on the assumed disk mass function and find that a higher parallax incidence is favored by mass functions with higher mean masses. Parallax measurements yield the reduced transverse speed, $\tilde{v}$, which gives both the relative transverse speed and lens mass as a function of distance. We give examples of the accuracies with which $\tilde{v}$ may be measured in typical parallax events. Fitting ML light curves, which may be shape-distorted (e.g., by parallax, blending, etc.), with only the three standard ML parameters can result in inferred values for these quantities that are significantly in error. Using our model, we study the effects of such systematic errors and find that, due primarily to blending, the inferred timescales from such fits, for events with disk lenses, tend to shift the event duration distribution by $\approx 10\%$ toward shorter $t_0$. Events where the lens resides in the bulge are essentially unaffected. In both cases, the impact parameter distribution is depressed slightly at both the low and high ends.

*Subject headings:* astrometry — Galaxy: general — gravitational lensing — stars: distances

## 1. INTRODUCTION

The recent observations by the MACHO (Alcock et al. 1995a, 1996a), EROS (Aubourg et al. 1993), OGLE (Udalski et al. 1994a), and DUO (Alard et al. 1995) collaborations of gravitational microlensing (ML) of stars in the LMC and Galactic bulge have generated tremendous excitement in astrophysics. These surveys provide a new probe of Galactic structure and low-mass stellar populations. ML observations of the LMC allow measurements of the dark matter content of the Galactic halo (Alcock et al. 1996a), placing important constraints on dark matter theories. Observations of ML events toward the Galactic center, which probe the inner disk and bulge of our Galaxy, have been intriguing as well; the roughly 100 events observed to date imply an optical depth toward the bulge of $(3.3 \pm 1.2) \times 10^{-6}$, 3 times that predicted by theoretical estimates (Griest et al. 1991), and reveal the need for a better understanding of Galactic structure.

One explanation for the observed excess of bulge events would be the presence of a hitherto undiscovered population of compact, substellar objects, implying the existence of more mass in the disk than previously believed (Alcock et al. 1995a; Gould, Miralda-Escude, & Bahcall 1994). This would require an upturn in the stellar mass function (MF) below the hydrogen-burning limit. Another possibility is that the lenses comprise an ordinary stellar population, and the enhancement of ML events is due to nonaxisymmetric structure, such as a bar, in the Galactic bulge. The optical depth calculated from a self-consistent bar model, matching both kinematic observations of the bulge and the *COBE* image of the Galaxy, is consistent with the MACHO and OGLE results (Kiraga & Paczyński 1994; Zhao, Spergel, & Rich 1995; Zhao, Rich, & Spergel 1996). Furthermore, the best-fit models to the observed ML duration distribution have a median lens mass of about 0.2 $M_\odot$, *above* the hydrogen-burning limit and consistent with ordinary stellar populations.

Determining the nature and location of the lenses will enable us to learn whether the enhancement of bulge events is due to lenses in the bar or in the disk, and to probe a region of the stellar MF about which little is known. However, while numerous cases of ML have been observed,

essential information such as the mass, distance, and velocity distributions of the lensing population can only be disentangled in a statistical manner, because of the degeneracy of microlensing light curves with respect to these parameters. For an ideal ML event, where the source and lens are assumed to be pointlike, the lens is assumed to be dark, and the velocities of the observer, source, and lens are constant, the amplification is given by

$$A[u(t)] = \frac{u^2 + 2}{u(u^2 + 4)^{1/2}}; \quad u(t) = \left[\left(\frac{t - t_{\max}}{t_0}\right)^2 + u_{\min}^2\right]^{1/2}, \tag{1}$$

where $u$ is the impact parameter from the observer-source line to the lens in units of the Einstein radius, $t_0 = R_E/v$ is the event timescale, $v$ is the transverse speed of the lens relative to the source-star line of sight, and $t_{\max}$ is the time at which peak amplification, $A_{\max} = A(u_{\min})$, occurs. The Einstein radius, $R_E$, is determined by the geometry of the event and the lens mass, and is given by

$$R_E = \left[\frac{4GM_l D_{ol}(D_{os} - D_{ol})}{c^2 D_{os}}\right]^{1/2}, \tag{2}$$

where $M_l$ is the lens mass, and $D_{ol}$ and $D_{os}$ denote the observer-lens and observer-source distances, respectively. We see from equation (1) that the ideal ML light curve can be fitted by the three parameters $t_0$, $t_{\max}$, and $u_{\min}$. The latter two, however, only tell when the lens passed nearest to the line of sight and how close it came, revealing little useful information about the event. All the parameters of interest, namely, $M_l$, $v$, $D_{ol}$, and $D_{os}$, are folded into the single parameter $t_0$. (In practice, $D_{os}$ may be obtained to reasonable accuracy.)

Several techniques for breaking the degeneracy have been proposed, many of which involve fitting for distortions to the generic ML light curve that may be detected in some fraction of observed events (Nemiroff & Wickramasinghe 1994; Witt & Mao 1994; Maoz & Gould 1994; Loeb & Sasselov 1995; Han & Gould 1995; Gaudi & Gould 1996). These distortions arise from violations of the standard ML assumptions. For example, if the lenses consist partly of ordinary, low-mass dwarfs in the Galactic disk and bulge, the contribution of the lens light in a given event would distort the observed light curve differently in different wave bands, violating the assumption of achromaticity and distorting the shape (cf. eq. [1]) of the light curve (Kamionkowski 1995; Buchalter, Kamionkowski, & Rich 1996, hereafter BKR). Ground-based observations of this color-shift effect in two or more wave bands can remove entirely the degeneracy in $t_0$. If the lenses are not completely dark, then color-shifting should, in principle, affect every event, and the observed incidence of this effect is simply a function of resolution of the data (namely, sampling frequency and level of photometric error). The MACHO collaboration has already observed another type of distortion, where the time symmetry of the light curve is broken by the Earth's orbital motion (Alcock et al. 1995b). This parallax effect allows one to compare the projected Einstein ring with the size of the Earth's orbit and thereby obtain an additional constraint relating $M_l$, $v$, and $D_{ol}$, effectively removing one degree of degeneracy. Strictly speaking, this effect is also present in every event but is not expected to be observed frequently by any of the existing ML surveys; the light curves are sampled too infrequently, and the photometric errors are too large. The single confirmed parallax event detected to date was fortuitous in that it was both long enough ($t_0 \approx 110$ days) for the light curve to be heavily sampled and well-situated during the MACHO observing season so that the asymmetry could be fitted along the entire light curve. In addition, the effect is more dramatic for longer events, during which the Earth can move through an appreciable fraction of its orbit. It is only for these rarer long events that a parallax shift may be observed by the low-resolution ML surveys. However, with the early-warning alert systems developed by both the MACHO and OGLE groups (Udalski et al. 1994b; Alcock et al. 1996b), it is conceivable that a program of follow-up observations with frequent and precise measurements could measure the light curves with sufficient accuracy to detect the parallax effect in a larger fraction of events. The PLANET (Albrow et al. 1996) and GMAN (Alcock et al. 1996c) collaborations are currently performing such observations, with the primary purpose of detecting planets around lenses. Planetary masses would give rise to smaller event timescales and thus produce narrow spikes on the lensing light curve that likely go undetected in current surveys. These spikes could be resolved with observations by dedicated telescopes performing rapid sampling of events in progress with high photometric precision (Peale 1996). Such ground-based surveys are well-suited to pick out the parallax effect for shorter term events, as well as distortions due to blended light from the lens or otherwise.

In this paper, we determine the fraction of ML events toward the Galactic bulge that should show a measurable parallax shift in such follow-up programs. We calculate the fractions that will arise if the lenses are all in the bulge and if the lenses are all in the disk, using realistic models for the lens distributions that are consistent with the currently observed ML timescale distribution. A Monte Carlo technique is used to simulate events and generate parallax-distorted light curves for each. It is then determined for each event whether the distorted light curve can be distinguished at the 95% confidence level from a standard ML light curve. The calculation is performed for several values of the sampling frequency and for several values of photometric accuracies that may be attainable. Our results indicate that, depending on the survey sensitivity, the expected fraction of parallax-shifted events ($F_{PSE}$) ranges from 0.06 to 0.31 for bulge self-lensing events, 0.31 to 0.77 for disk-lensing–bulge events, and 0.49 to 0.83 for (rare) disk self-lensing events, with the current generation follow-up surveys favoring the lower values. Since the parallax effect is important for the case of disk lenses particularly, we also examine the dependence of this effect on the adopted MF for the disk and find higher incidences from MFs with higher mean masses. We further calculate the dependence of $F_{PSE}$ on the event timescale, finding that the intensive follow-up programs should measure a substantial contribution to $F_{PSE}$ from events with $t_0$ as low as 20 days, and we also examine what may be learned from a typical parallax-shifted event (PSE). We emphasize that, like color-shift analysis, parallax analysis can be applied directly to all events, so that information about the mass, velocity, and spatial distributions of the lenses becomes available on an event-by-event—rather than on a statistical—basis.

Although parallax and blending effects may be present to some degree in a large fraction of events, they are expected to be small in most cases, so that a standard three-parameter fit to a slightly distorted light curve may be

deemed adequate. However, fitting the standard ML amplification function to a light curve distorted by these effects can result in systematic errors in the inferred fit parameters, most notably $t_0$ and $u_{\rm min}$. These inaccuracies may lead to a systematic miscalculation of the duration and amplification distributions and of the overall optical depth. Thus, we perform another simulation in order to generate shape-distorted light curves, including both parallax and color-shift effects (i.e., blending due to the lens). A standard three-parameter fit to these light curves is then applied, and the inferred parameters are used to compare the resulting amplification and event duration distributions with their actual values. For the latter, we find that the errors incurred by three-parameter fits are negligible for bulge lenses but may be quite large ($\geq 10\%$) if the lenses are in the disk, particularly if the disk MF declines at the low-mass end. We also find that errors in the inferred minimum impact parameter lead to a nonuniform distribution in peak amplification.

The plan of the paper is as follows. In § 2, we review the characteristics of parallax-distorted events. In § 3, we summarize the models and techniques used in the calculation and present the results of our calculations of the expected fraction of PSEs. In § 4, we examine the impact of parameterizing shape-distorted light curves with the standard ML fit on the inferred ML parameters, and in § 5 we make some concluding remarks.

## 2. PARALLAX-SHIFTED MICROLENSING EVENTS

To parameterize the parallax effect, let us consider first a standard ML event as viewed at the position of the Sun. In that case, we regain the constant-velocity condition, so that the scaled distance from the lens to the line of sight, $u(t)$, is properly described by equation (1), where $u_{\rm min}$ now represents the minimum distance from the lens to the Sun-source line of sight. We can modify the expression for $u(t)$ to incorporate the Earth's orbital motion by projecting to the position of the lens the motion of the observer (Earth) along the ecliptic. Figure 1 depicts a simplified version of the geometry, where we have assumed, for the sake of illustration, that the ecliptic is perpendicular to the Sun-source line. In this case, we see from Figure 1*a* that the projection of the Earth's orbit traces out a circle with a radius (scaled in units of $R_{\rm E}$) given by

$$\alpha = \frac{a}{R_{\rm E}} = \frac{R_\oplus}{R_{\rm E}}\,(1 - x)\,, \tag{3}$$

where $R_\oplus = 1$ AU and $x = D_{\rm ol}/D_{\rm os}$. Figure 1*b* shows a cross section of the parallax cone in Figure 1*a*, taken at the position of the lens. The projected motion of the Earth at the lens position is given by $\boldsymbol{r}_\oplus(t) = \{\alpha \cos [\Omega(t - t_c)], \alpha \sin [\Omega(t - t_c)]\}$. In actuality, we must account for the true orientation of the ecliptic with respect to the Galactic plane. The true projection of the Earth's orbit is an ellipse whose eccentricity is determined by the ecliptic latitude, $\beta$, of the source, so that

$$\boldsymbol{r}_\oplus(t) = \{\alpha \sin \beta \cos [\Omega(t - t_c)], \alpha \cos \beta \sin [\Omega(t - t_c)]\} \tag{4}$$

is the correct expression. For stars in Baade's window ($l = -1°$, $b = 4°$), $\beta \approx 4°$, so $\cos \beta \approx 1$. The parameter $\Omega$ is

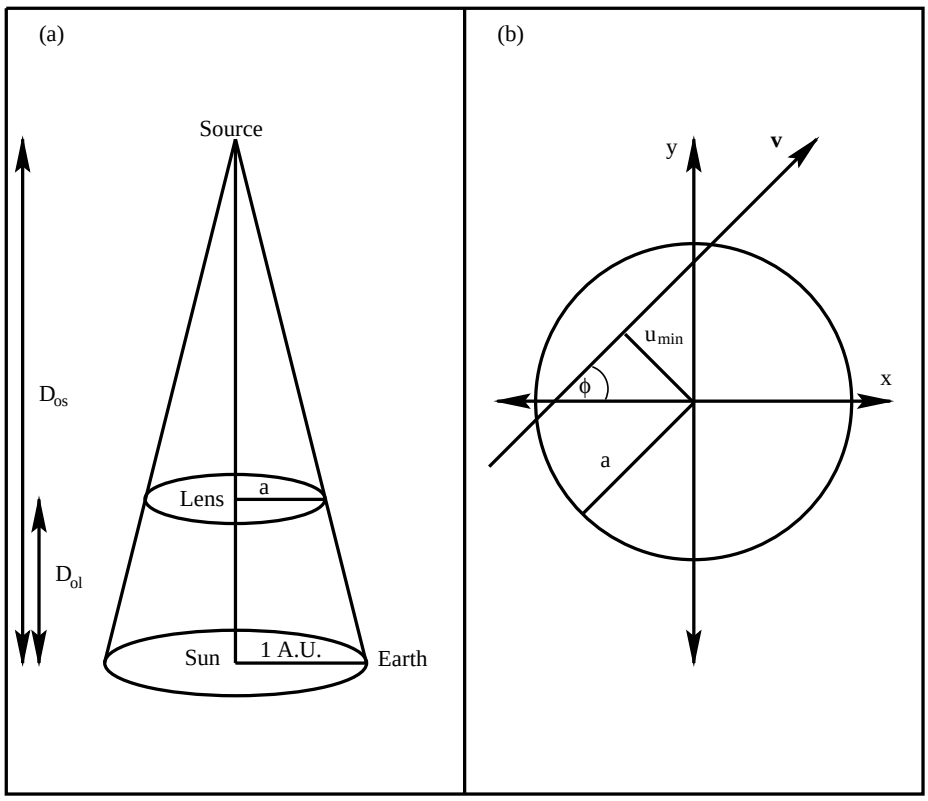


FIG. 1.—(*a*) Simplified geometry of the parallax cone, assuming the ecliptic is perpendicular to the Sun-source line. The Earth's orbit, projected to the position of the lens, traces out a circle of radius *a*. (*b*) Cross section of the parallax cone at the distance of the lens. The lens velocity is denoted by $\boldsymbol{v}$. Note that $u_{\rm min}$ is no longer the minimum distance from the lens to the observer-source line of sight, but rather the distance from the lens to the Sun-source line of sight.

given by

$$\Omega(t - t_c) = \Omega_0(t - t_c) + 2\epsilon \sin [\Omega_0(t - t_p)] , \quad (5)$$

where $t_c$ is the time when the Earth is closest to the Sun-source line, $\Omega_0 = 2\pi$ yr$^{-1}$, $t_p$ is the time of perihelion, and $\epsilon = 0.017$ is the eccentricity of Earth's orbit. We include the dependence on $\epsilon$ in our expression for $\Omega$ since it may contribute appreciably near $t = t_c$, although we omit it in the expression for $\alpha$, where it is always negligible. The position of the lens is given by Figure 1*b* as

$$\begin{aligned} \boldsymbol{r}_{\rm lens}(t) = [&-u_{\rm min} \sin \phi + v(t - t_{\rm max}) \\ &\times \cos \phi, u_{\rm min} \cos \phi + v(t - t_{\rm max}) \sin \phi] , \end{aligned} \quad (6)$$

where $\phi$ denotes the angle between $\boldsymbol{v}$ and ecliptic north. Using $\omega = t_0^{-1}$, we thus have

$$\begin{aligned} u^2(t) &= (x_{\rm lens} - x_\oplus)^2 + (y_{\rm lens} - y_\oplus)^2 \\ &= u_{\rm min}^2 + \omega^2(t - t_{\rm max})^2 \\ &\quad + \alpha^2 \sin^2 [\Omega(t - t_c)] + \alpha^2 \sin^2 \beta \cos^2 [\Omega(t - t_c)] \\ &\quad - 2\alpha \sin [\Omega(t - t_c)][\omega(t - t_{\rm max}) \sin \phi + u_{\rm min} \cos \phi] \\ &\quad + 2\alpha \sin \beta \cos [\Omega(t - t_c)] \\ &\quad \times [u_{\rm min} \sin \phi - \omega(t - t_{\rm max}) \cos \phi] , \end{aligned} \quad (7)$$

so that a parallax-shifted light curve is parameterized by the five quantities $t_{\rm max}$, $t_0$, $u_{\rm min}$, $\alpha$, and $\phi$. In our simulations, we include an additional parameter to account for the presence of unlensed light (either due to the lens or a chance blended star) in the light curve.

Figure 2 illustrates an example of a ML light curve distorted by the parallax effect. The solid curve is a simulated PSE, arising from a bulge self-lensing configuration with $t_0 = 100$ days and $\alpha = 0.13$. The dashed curve is a standard ML curve with the same peak height ($A_{\rm max}$), peak time ($t_{\rm max}$), and FWHM, and a timescale of $t_0 = 97$ days. It is important to note that since the two curves have different shapes, as indicated by the residuals in the lower panel, a fit to a PSE that involves only the parameters $t_{\rm max}$, $t_0$, and $u_{\rm min}$ can generate inferred values of these quantities that are significantly in error. This is further evidenced by the MACHO collaboration analysis of their PSE, in which they find the best-fit standard curve to have $t_0 = 141$ days and $u_{\rm min} = 0.101$, and the best-fit parallax curve to have $t_0 = 111$ days and $u_{\rm min} = 0.159$ (Alcock et al. 1995b). Failing to account for distortions in observed ML light curves can lead to errors in the inferred timescales and thus in the inferred optical depth as well.

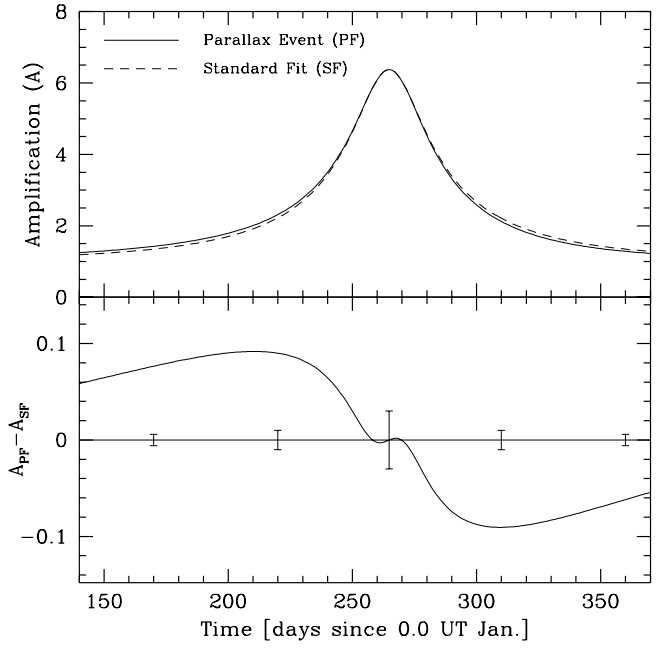


FIG. 2.—The upper panel shows a parallax-shifted light curve (*solid line*) for an event arising from a 0.3 $M_\odot$ object at 6 kpc (i.e., the near end of the bulge) lensing a source at 8 kpc. This curve has the values $\alpha = 0.13$ and $t_0 = 100$ days. A standard ML light curve (*dashed line*), with identical $A_{\rm max}$, $t_{\rm max}$, and FWHM, has a value of $t_0 = 97$ days. The residuals in the lower panel illustrate the time asymmetry of the parallax effect in this event.

## 3. EXPECTED FRACTIONS OF PARALLAX-SHIFTED EVENTS

To calculate the expected fraction of ML events toward Baade's window that will give rise to a measurable parallax shift, we employ the method used by BKR in a similar calculation of expected rates for color-shifted events. The Galactic model consists of a rapidly rotating bar extending out to 3 kpc (Zhao 1996) and a double exponential disk, extending from 3 kpc out to the solar circle, with a rotational velocity of 220 km s$^{-1}$ coupled with position-dependent velocity dispersions of order 30 km s$^{-1}$. Both components are populated by stars following a logarithmic MF in the range $0.1\ M_\odot \le M_l \le 1.2\ M_\odot$. These distributions produce an event duration distribution that is consistent with observed ML timescales (see BKR, Fig. 3), although other evidence points toward a disk MF that exhibits some flattening below 1 $M_\odot$ (Scalo 1986; Larson 1986; Gould, Bahcall, & Flynn 1996).

Using this model, we wish to predict the incidence of PSEs that would be observed by the follow-up programs described above. We parameterize various observing strategies by the time interval between successive measurements and by the level of photometric error. Since a constant error in magnitude translates into a constant percent error in amplification, we assume that any given value of $A$ has a Gaussian distribution centered at the true value with root variance $\sigma_i \approx fA(t_i)$ that is some fraction $f$ of the true amplification, as determined by the assumed magnitude error. To determine whether a shape distortion in a given event will be observable, we first simulate the expected observed amplification with light-curve measurements for a given sampling frequency and fractional error, and then ask whether the six-parameter fit can recover a value of $\alpha$ that is different from zero at the 95% (2 $\sigma$) confidence level. If $\alpha$ differs from zero with this statistical significance, then a shape distortion from the parallax effect has been observed. All events were weighted by the frequency corresponding to their timescale, $t_0$ (see BKR, § 4), and summed to give an overall normalization. The fraction of parallax-shifted events, $F_{\rm PSE}$, is defined as the ratio of the weighted sum of all PSEs to the overall normalization. In our calculations, we adopt the OGLE detection efficiency, given by $\epsilon(t_0) = 0.3$ exp $[-(t_0/11\ \text{days})^{-0.7}]$ (Udalski et al. 1994a). The MACHO efficiencies are typically higher for a given event duration (Alcock et al. 1996a) but do not alter significantly our results for parallax-shifting.

In determining $F_{\rm PSE}$, we consider separately the case of bulge self-lensing (BB), disk objects lensing bulge sources (DB), and disk self-lensing (DD). Although the disk lensing events contribute less to the overall optical depth (particularly in the case of disk self-lensing), the lower trans-

verse speed of the disk lenses will give rise to longer duration events whose light curves will be heavily sampled and thus more likely to yield a parallax shift. Our light-curve analysis for each event included data from the time, $t_s$, at which the amplification rose above threshold [i.e., $A(t_s) = A_T = 1.34$] until $3t_0$ after the amplification dropped below threshold. Our results indicate that additional data out to $3t_0$ give rise to a considerable increase in $F_{\rm PSE}$ compared with data taken only while $A \geq A_T$, since the effects of parallax distortion may be significant away from the peak; extending the data out to $7t_0$, however, does not appreciably increase $F_{\rm PSE}$ beyond the $3t_0$ value. Our simulations included only those events in which the event timescale $t_0$ satisfied $t_0 \leq 1$ yr. For each event, a $u_{\rm min}$ was chosen randomly in the range $0 < u_{\rm min} < 1$. If, however, the experimental efficiency for detecting low-amplification events is small, so that the effective range of $u_{\rm min}$ is, say, from 0 to 0.7 (Alcock et al. 1996a; Gaudi & Gould 1996), then the fraction of parallax-shifted events would increase since the effect becomes more pronounced at higher amplifications.

Figure 3 displays the results of our calculation, showing $F_{\rm PSE}$ as a function of sampling interval, for the various lens/source configurations. The solid, short-dashed, and long-dashed curves represent photometric errors of 0.05, 0.01, and 0.001 mag, respectively. The results indicate that current surveys, which sample roughly daily with typical errors of order 0.05 mag, are not expected to yield many PSEs. For these observational parameters, about 1% of all events should exhibit a detectable parallax shift, consistent with the one PSE observed by the MACHO collaboration out of a total of about 100 bulge events to date. However, the figure shows significant increases in $F_{\rm PSE}$ for decreased sampling intervals, and lower levels of photometric error. For the most likely case of BB, hourly sampling with 0.01 mag errors, typical of the PLANET experiment, gives $F_{\rm PSE} = 0.06$, increasing to 0.10 for 15-minute sampling. In the case of DB lensing, these numbers increase to 0.31 and 0.42, respectively. Together, these imply an overall expected parallax-shifting rate of 10% for hourly sampling and 15% for 15-minute sampling (assuming $\tau_{\rm DB} \approx \frac{1}{5}\tau_{\rm BB}$ and neglecting $\tau_{\rm DD}$). Depending on their capabilities, current planetary surveys are thus expected to detect parallax effects in roughly 10%–15% of all events. It is, however, conceivable that future experiments with high-precision relative photometry from additional dedicated telescopes can produce errors in the millimagnitude range (Gilliland et al. 1993; Ciardullo & Bond 1996). Differencing techniques have already been used to achieve extraordinary precision in pixel lensing experiments (Crotts & Tomaney 1996). To illustrate what may be learned by such experiments, we also consider the results from millimagnitude errors. Together with a rapid sampling rate, this improvement could bring the expected $F_{\rm PSE}$ as high as 0.31 for BB events and 0.77 for DB events, for a maximum overall rate of 39%. In general, events arising from a DD configuration are expected to be rare, since $\tau_{\rm DD}$ is only about $5 \times 10^{-3}\tau_{\rm BB}$. Owing to their low relative transverse speeds, however, any DD events observed will have a high likelihood of exhibiting the parallax effect. Indeed, for 0.01 mag errors, $F_{\rm PSE} = 0.49$ for hourly sampling, increasing to 0.59 for 15-minute sampling. It should be noted that if the unlensed-light parameter is neglected in the fitting procedure, the above values for $F_{\rm PSE}$ in the different scenarios increase substantially, doubling in some cases. The unlensed-light parameter in each wave band introduces another degree of freedom in the fit, which drives down $F_{\rm PSE}$. Since we have no a priori knowledge of the extent to which a given observed ML light curve is distorted by these different effects, it is important to include the possible contribution of blended light in the fit.

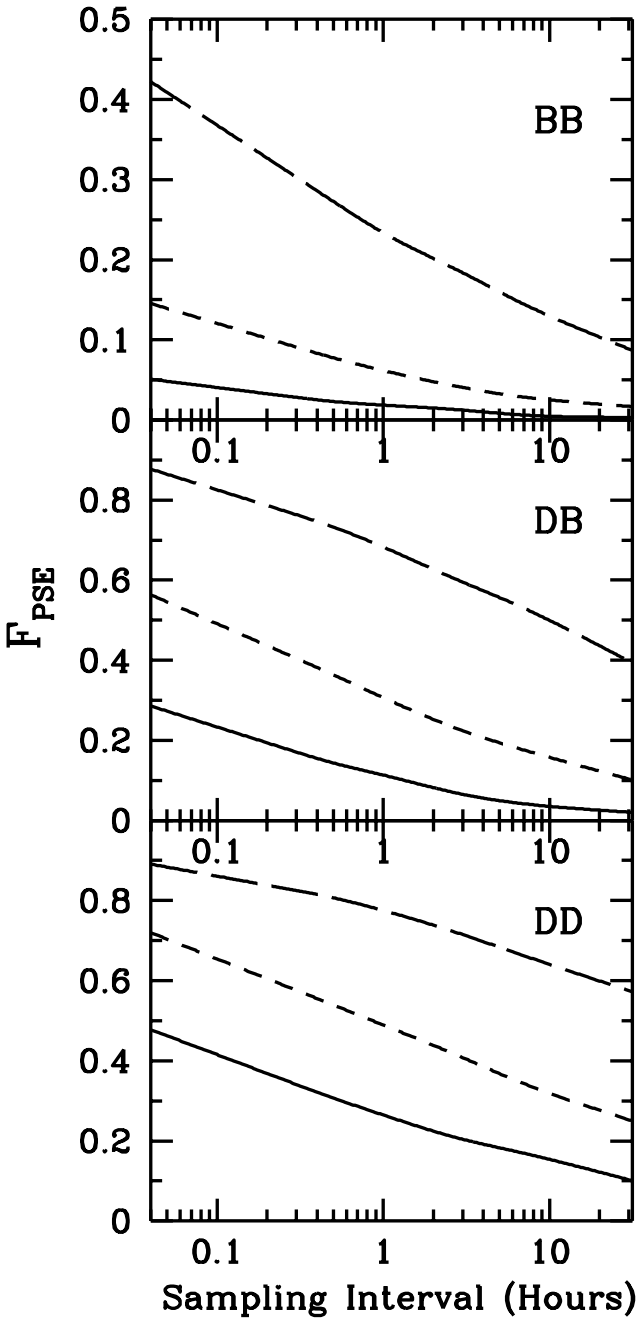


FIG. 3.—Expected fraction of PSEs as a function of sampling interval. The solid, short-dashed, and long-dashed curves correspond to photometric errors of 0.05, 0.01, and 0.001 mag, respectively. The various configurations are denoted by BB for bulge self-lensing, DB for disk-lensing–bulge events, and DD for disk self-lensing.

In Figure 4, we plot $F_{\rm PSE}$ as a function of $t_0$ for the three lens/source configurations, assuming 0.5 hr sampling with 0.005 mag errors (*upper curves*) and daily sampling with 0.05 mag errors (*lower curves*). It is clear from the figure that the intensive follow-up programs will provide a vast improvement over the existing large surveys in detecting parallax distortions, not only for the longest duration events but for

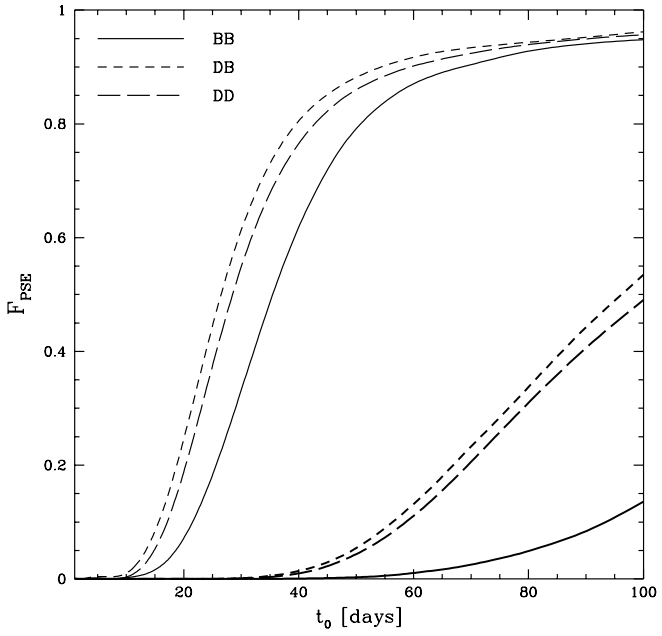


FIG. 4.—$F_{PSE}$ as a function of $t_0$ for the BB, DD, and DD configurations. The upper curves are the results from simulated data with 0.5 hr sampling and 0.005 mag errors, illustrating what may be achieved by intensive follow-up programs. The lower curves show the results from data taken daily with 0.05 mag errors, typical of MACHO and OGLE experiments.

all events with timescales $t_0 \geq 10$ days. Moreover, the figure shows that the parallax effect is more pronounced for events in which the lens resides in the Galactic disk (i.e., DB and DD). This is due to two factors: the lower transverse speeds arising from our corotation with disk lenses give rise to longer duration events that can be heavily sampled along a larger fraction of the Earth's orbit (affecting DB and DD), and the typical separations between disk stars (lenses) and bulge stars (sources) give rise to a more favorable parallax geometry (affecting DB only) (see Fig. 1). For 0.5 hr sampling with 0.005 mag errors, $F_{PSE}$ for BB events becomes appreciable for timescales of $t_0 \geq 20$ days, reaching 0.5 near $t_0 = 35$ days, while for DB events $F_{PSE}$ becomes appreciable for $t_0 \geq 15$ days, reaching 0.5 at $t_0 = 26$ days. Note that while the overall $F_{PSE}$ is greater for DD events, as in Figure 3, the fraction as a function of $t_0$ is lower, especially for smaller $t_0$, because the duration distribution for DD events is shifted toward higher $t_0$, owing to their lower relative transverse speeds.

In the above calculations, we assumed a logarithmic MF down to 0.1 $M_\odot$ for disk lenses, which is consistent with current ML observations. However, other evidence points to a disk MF that turns over at masses near 0.4 $M_\odot$ (Scalo 1986; Larson 1986; Gould et al. 1996). Thus, given the sensitivity of $F_{PSE}$ to disk lenses, we also consider the *Hubble Space Telescope* (*HST*) MF, $\log \phi = 1.35 - 1.34 \log (M/M_\odot) - 1.85 [\log (M/M_\odot)]^2$ in the range $0.1\ M_\odot \leq M_l \leq 5.0\ M_\odot$, as well as a composite power-law MF with $dN/dM = 0$ for $0.1\ M_\odot \leq M_l \leq 0.4\ M_\odot$, $dN/dM \propto M^{-1.25}$ for $0.4\ M_\odot \leq M_l \leq 1.0\ M_\odot$, $dN/dM \propto M^{-2.3}$ for $1.0\ M_\odot \leq M_l \leq 3.0\ M_\odot$, and $dN/dM \propto M^{-3.2}$ for $3.0\ M_\odot \leq M_l \leq 5.0\ M_\odot$ (Mihalas & Binney 1982). The *HST* MF has a higher mean mass than the logarithmic MF, and the composite power-law MF favors still higher masses. The results for these MFs are compared with our previous results in Figure 5. Parallax effects are seen to be quite sensitive to the disk MF, becoming more dramatic with higher mean masses, and, like color shifts, may be used as a means to discriminate between different forms for the stellar MF.

In the preceding discussion, we have not focused on the results from a particular survey but rather have considered a broad spectrum of observational capabilities, some of which are outside the range of current surveys. For example, 15-minute sampling with 1% $V$-band photometry of a $V = 21$ star in Baade's window during a full moon with 1″ seeing would require a 3 m telescope for the follow-up surveys. Photometric errors will depend generally on the source brightness, and the details of any given experiment are governed ultimately by systematics, such as seeing variations, varying aberrations, and telescope alignment errors, that will require more detailed modeling. Our results for the fraction of observably distorted events arise from the parameterization of an idealized survey and are intended as a template for comparison with various observational assumptions. For example, if the above systematic errors give rise to night-to-night variations in the photometry that are of order 0.01 mag (larger than the assumed statistical errors), a lower limit to $F_{PSE}$ could be attained by assuming a degraded photometric error of 0.01 mag (the magnitude of the nightly errors) and a degraded sampling frequency of one per day. In this case, Figure 3 predicts fractions of 2% and 11% for BB and DB lensing, respectively, for an overall rate of about 4%. It should be noted, however, that dedicated ground-based instrumentation taking continuous and redundant measurements from multiple sites, together with possible space-based observations, should help control such effects. Moreover, since it is the source amplification, and not absolute brightness, that is essential, calibration against nonvariable sources in the survey may also help reduce the effects of long-term drifts. As mentioned above, techniques involving relative photometry are capable of yielding high-precision measurements, particularly if coupled with space-based observations to provide a stable reference frame.

Depending on the particular capabilities of the microlensing follow-up surveys, 10% or more of all events observed toward the bulge are expected to have a detectable parallax shift at the 95% confidence level. Such events can yield valuable information about the properties of the lens (Alcock et al. 1995b). In particular, since

$$\alpha = \frac{R_\oplus}{R_E}(1 - x) = \frac{\omega R_\oplus}{v}(1 - x)\,, \tag{8}$$

measurements of $\alpha$ and $\omega$ allow the determination of the reduced transverse speed $\tilde{v} = v/(1 - x) = \omega R_\oplus/\alpha$, giving $v$ as a function of $x$ (or $D_{ol}$, if $D_{os}$ is known). In our simulation, analysis of the covariance matrix of the six-parameter fit (see BKR) yields the standard errors in $t_0 = \omega^{-1}$ and $\alpha$ for a given event, thus determining the error in $\tilde{v}$. As a simple illustration of the accuracies that may be attained, we simulated the light curves of events with typical BB and DB configurations, i.e., a 0.3 $M_\odot$ lens at 6 kpc (the near end of the bulge) and 4 kpc, respectively, lensing a source at 8 kpc, with $u_{min} = 0.2$, $\phi = 1$ rad, and $t_{max}$ on June 1. The resulting 1 $\sigma$ limits on $\tilde{v}$, for various timescales and observational parameters, are shown in Table 1. While the best results are obtained for the longest duration events, useful constraints can be obtained for shorter duration events ($t_0 \approx 1$ month) as well.

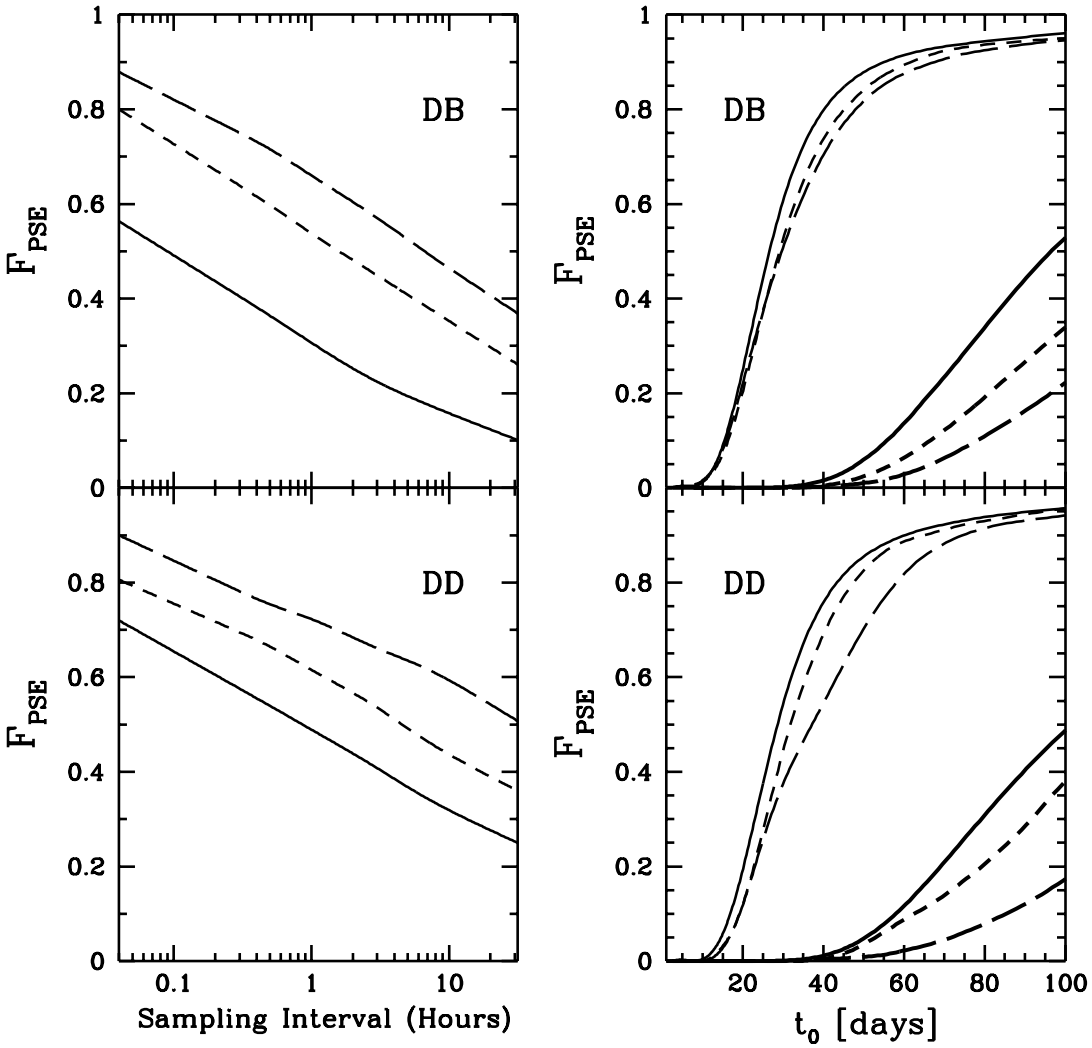


FIG. 5.—Variations in $F_{PSE}$ arising from different disk MFs. The solid, short-dashed, and long-dashed curves correspond to the logarithmic, *HST*, and composite power-law MFs, respectively. The left panels depict the expected fraction of PSEs as a function of sampling interval, assuming 0.01 mag errors. The panels on the right show $F_{PSE}$ as a function of $t_0$, where the thin lines correspond to 0.5 hr sampling with 0.005 mag errors and the thick lines correspond to daily sampling with 0.05 mag errors. Note that while the overall fractions increase with higher mean lens masses, the fractions as a function of $t_0$ are lower because the higher masses give rise to longer event timescales.

TABLE 1

ESTIMATED ACCURACIES $\Delta\tilde{v}/\tilde{v}$ (1 $\sigma$ LIMITS)

| $t_0$ (days) | 1 hr, 0.01 mag | 0.5 hr, 0.005 mag |
|---|---|---|
| | BB | |
| 15..... | 2.25 | 0.79 |
| 30..... | 0.29 | 0.10 |
| 60..... | 0.04 | 0.01 |
| | DB | |
| 15 ..... | 1.33 | 0.47 |
| 30 ..... | 0.17 | 0.06 |
| 60 ..... | 0.03 | 0.01 |
| 100..... | 0.01 | 0.004 |

NOTE.—Estimated 1 $\sigma$ accuracies for measurements of $\tilde{v}$ from the simulated BB and DB events, for various event timescales, $t_0$. The results from simulated data taken with hourly sampling and 0.01 mag errors, and from 0.5 hr sampling and 0.005 mag errors, are shown. Note that useful accuracies are achieved even for events with $t_0 \approx 30$ days.

Gaudi & Gould (1996) have performed a similar calculation for PSEs observed simultaneously from the Earth and by a satellite in heliocentric orbit, and they find that for photometric precisions of 1%–2%, such observations could measure $\tilde{v}$ to an accuracy of $\leq 10\%$, at the 1 $\sigma$ level, for over 70% of disk lenses and for over 60% of bulge lenses. Adopting their $u_{\rm min}$ distribution, we find that for hourly sampling and 1% photometric precision (typical of the PLANET data), ground-based observations of the parallax effect will measure $\tilde{v}$ to this accuracy in only 2% of all BB events and 14% of all DB events, indicating that satellite measurements would provide considerable improvement.

Parallax-shift analysis provides a constraint between $v$ and $x$ that removes one degree of degeneracy from $t_0$; knowledge of $\tilde{v}$ also allows one to express $M_l$ in terms of $x$. In particular,

$$t_0 = \frac{R_{\rm E}}{v} = \frac{\sqrt{4GM_l x(1-x)D_{\rm os}/c^2}}{\tilde{v}(1-x)}$$

$$\Rightarrow M_l(x) = \frac{\tilde{v}^2 t_0^2 c^2}{4GD_{\rm os}} \frac{1-x}{x}. \quad (9)$$

Moreover, knowledge of $\phi$ provides additional information about the direction of the relative transverse velocity that can be useful in distinguishing between lenses belonging to bulge and disk populations. Such constraints can be used in conjunction with those obtained from other independent analyses, such as deviations from the point-source approximation, or the analysis of blending effects.

## 4. CORRECTIONS TO MICROLENSING DISTRIBUTIONS

We have already seen that if a shape-distorted event is fitted with the standard three-parameter curve, the inferred values of $u_{\min}$, $t_{\max}$, and $t_0$ can be appreciably in error (Alcock et al. 1995b; BKR). While the first two are essentially random variables and do not affect our understanding of the lens distributions, the event timescale, $t_0$, is critical, and any discrepancy in this value will propagate into the assumed values for the lens distributions and the overall optical depth. In principle, every ML event is parallax-shifted and (if the lenses are not assumed to be totally dark) color-shifted; even if the lens is dark, the observed light curve may be distorted by blended light from an optical companion (Di Stefano & Esin 1995). While such effects are important in that they allow us to derive more information from an event than is otherwise possible, and while both effects may, in some fraction of events, be highly pronounced, in practice we find that their magnitude is usually small. In the case of blending, this is simply because one is usually searching for the small contribution of a faint star (possibly the lens) to the amplified light of a brighter star. For the parallax effect, the typical mass range of the lenses, together with the microlensing geometry toward the bulge, conspire to make $\alpha$ typically small. The degree to which these effects are observed is primarily a function of the resolution of the data, and many of the current surveys are not capable of detecting them. Thus, we wish to examine whether any systematic errors are incurred by routinely applying standard three-parameter fits to ML light curves that are allowed to suffer both parallax and blending distortions. To do this, we once again employ a Monte Carlo simulation of lensing events, using the Galactic model described in BKR. The shape distortion in a given event (parameterized by $\alpha$ and the luminosity offset ratio $r$) is determined by the masses and distances of the source and lens; the parallax effect is modeled as described above, and for simplicity, blending is assumed to be due to unlensed light from the lens, following the model of BKR. This assumption reflects an upper limit to the impact of blending, since the lens is located nearer to us than an optical companion is likely to be, thus appearing brighter, and it assumes blending occurs in every event. Each such light curve is generated and then fitted for only the three standard parameters to yield $t_0^{\rm inf}$, $t_{\max}^{\rm inf}$, and $u_{\min}^{\rm inf}$, where the superscripts distinguish these inferred values from the actual values (no superscript) used to generate the events. Due to the presence of $\alpha$ and $r$, the inferred values will generally differ from the actual ones, so that the inferred distributions of impact parameters (i.e., peak amplifications) and timescales will be different than their actual values. The model we employ is simply intended to give an estimate of the expected magnitude of such deviations.

Before turning to the calculations, it is instructive to make some brief qualitative observations about the expected differences between the inferred and actual quantities. The parallax effect is essentially a low-amplitude, sinusoidal-type variation superimposed on $u(t)$. On average, it should not push either the peak amplification (given by $u_{\min}$) or the event timescale, $t_0$, in any particular direction, since the correction to $u(t)$ in equation (8) can be positive or negative. Blending distortions (arising from the lens or otherwise), however, do operate preferentially. Let us suppose the light from an unresolved star (possibly the lens) with apparent brightness $l_*$ is blended with that of a source with a baseline brightness $l_s$. If the amplification of the background star is $A$, then the observed brightness is $l_{\rm obs} = l_* + Al_s$; the baseline brightnesses are obtained by setting $A = 1$. Due to the contribution of the unlensed light, the *observed* amplification, which we denote by $\mathscr{A}$, is different from the microlensing amplification $A$. The observed amplification in a given wave band will be

$$\mathscr{A}(t) = \frac{l_* + A(t)l_s}{l_* + l_s} = (1 - r) + A(t)r \,, \tag{10}$$

where $r = l_s/(l_s + l_*)$ is the luminosity offset ratio. The presence of $r$ distorts the shape of the observed light curve, even if the two stars have the same color. In the case of no blending, $r = 1$, and we recover the standard ML scenario. If there is *any* blended light, however, $r$ decreases. It can be shown easily that the observed amplification $\mathscr{A}$ is a monotonically decreasing function of $r$, so that all blended events exhibit an amplification that is everywhere less than that which would have been observed in the absence of blending. It follows that $u_{\min}^{\rm inf} > u_{\min}$ for all blended events. Since an event is only registered when the *observed* amplification exceeds threshold, the reduction in amplification translates into a shorter event duration and thus a smaller timescale, $t_0$. In particular, an event will be registered only while $\mathscr{A} > 1.34 \Rightarrow A \geq A_{\rm thresh} = [1.34 - (1 - r)]/r$, or only when the dimensionless lens–line-of-sight distance is $u \leq u_{\rm thresh} = u(A_{\rm thresh})$, where $u_{\rm thresh} < 1$. The observed event duration, $t_e = 2t_0[u_{\rm thresh}^2 - u_{\min}^2]^{1/2}$, is thus shorter than the no-blending case (where $u_{\rm thresh} = 1$), leading to a decrease in the inferred $t_0$. Thus, from blending effects, we expect to see the inferred duration distribution shifted toward shorter timescales. Moreover, since the blended stars are presumably low-mass dwarfs that emit most of their light at redder wavelengths, $r$ will decrease with increasing wavelength, so the reduction in amplification and in event timescale, in principle, should be more pronounced for longer wavelengths.

In Figure 6, we plot the smoothed, nonnormalized duration distribution, $d\Gamma/dt_0$, for BB and DB events, where we have again adopted the OGLE efficiency, $\epsilon(t_0)$. The solid curves are the actual values, and the dashed curves are the results from the inferred timescales from simulated distorted events with main-sequence (MS) source stars observed in $V$, allowed to suffer both parallax and blending effects. All curves assume a logarithmic disk MF. For BB events, there is no appreciable difference between inferred and actual distributions. Essentially, this is due to the shape of the bulge MF, which favors very low mass lenses, and the $V = 21$ mag cutoff for resolved sources. As a result, only the brightest MS bulge stars (near our upper mass cutoff) are lensed in our model, and the distortions from the distant, low-mass blended stars are too small to alter the timescales systematically. The same result would obviously hold true in the case of giant sources. For DB events, however, the lenses are

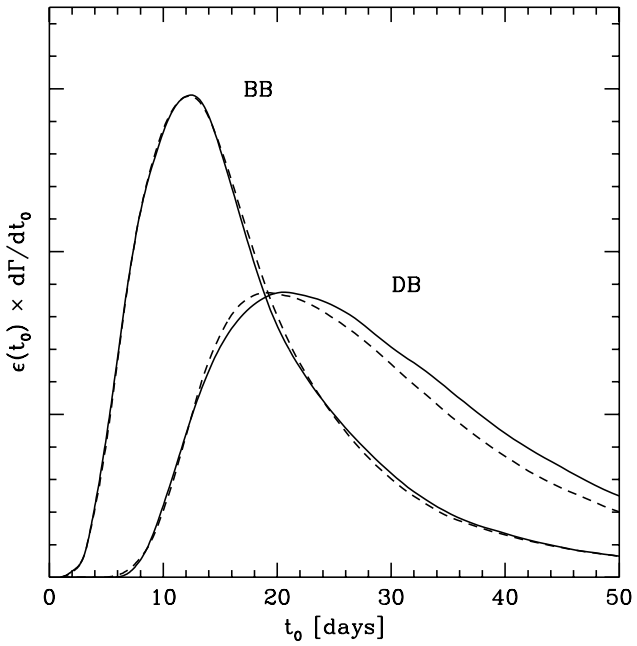


FIG. 6.—Nonnormalized ML event duration distributions for the bulge and disk models used. The solid lines are the results obtained using the actual event timescales $t_0$, while the dashed lines show the results obtained using $t_0^{\rm inf}$ from a standard fit to a blended event. The BB distribution (which matches the peak of the combined MACHO and OGLE data) is unaffected, but the DB distribution is shifted by about 10% toward smaller $t_0$.

closer to the solar circle, and their light contributions can become significant. Thus, for the DB curve, we find that for $t_0 > 14$ days, the distribution is shifted by roughly 10% along the entire curve toward shorter $t_0$. Our calculations also show that for the flatter disk MFs, which favor slightly higher masses, the change becomes more dramatic ($\approx$20% for the *HST* MF and $\approx$40% for the composite power-law MF), affecting even events with giant sources. DD events (not shown) show a similar behavior, although to a lesser degree than DB events, since the sources are so much nearer as well. We also ran a simulation in which events were distorted only by parallax and found no significant difference between observed and actual distributions, confirming that the shift seen in the figure is due to blending.

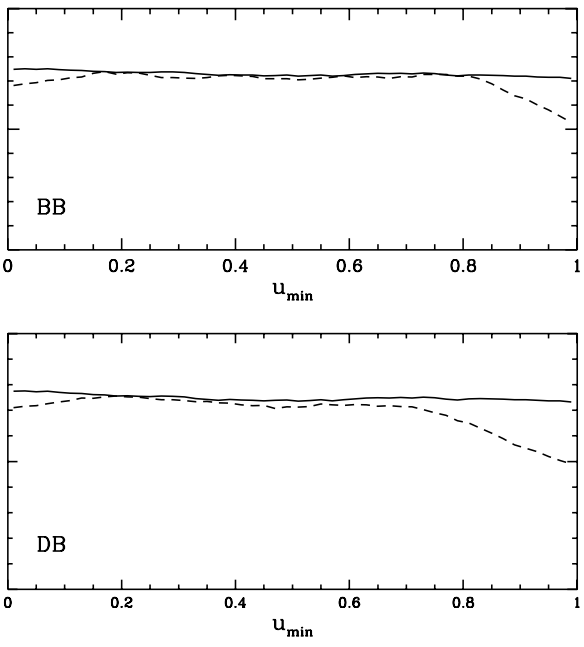


FIG. 7.—Nonnormalized number histogram of the impact parameter distribution for BB events (*upper panel*) and DB events (*lower panel*) observed in $V$. The solid lines show the (approximately uniform) distributions of the actual values ($u_{\rm min}$), while the dashed lines show the distributions of the inferred values ($u_{\rm min}^{\rm inf}$). The latter are nonuniform due to blending effects.

In addition to altering the duration distribution, the errors in $t_0$ also propagate into the optical depth, $\tau$, tending to *reduce* the inferred value of $\tau$ as well. However, an exact determination of both $d\Gamma/dt_0$ and $\tau$ requires an additional correction to account for the discrepancy between assumed and actual values of the source number density. Since a given blended source may actually be two or more unresolved sources, the inferred optical depth will be *enhanced* relative to the actual value as a result, and $d\Gamma/dt_0$ may be affected as well, although it is unlikely that events would be made longer. A precise calculation of blending effects requires a detailed model employing the frequency and separation distributions of optical binaries along the line of sight, and this is beyond our present scope. The above results are meant only to illustrate the impact of some of these effects.

Since $u_{\rm min}$, the impact parameter in units of $R_{\rm E}$, is a random variable, the distribution of $u_{\rm min}$ from an ensemble of events (expected to be uniform from 0 to 1) is used as a statistical check on microlensing. Due to blending effects, however, the distribution of $u_{\rm min}^{\rm inf}$ will not be uniform. First, since blending always causes a reduction in the observed amplification, the inferred impact parameter will be greater than its actual value in every blended event, resulting in fewer $u_{\rm min}^{\rm inf}$ at low values. However, there will be a decrease at high values also, because blended events where $u_{\rm min} > u_{\rm thresh}$ (recall $u_{\rm thresh} < 1$ in blended events) will never register. These effects are seen in Figure 7, which shows the nonnormalized inferred and actual $u_{\rm min}$ number distributions for both BB and DB events. We again assume observations in $V$ and a logarithmic disk MF. Detection efficiencies have not been included, although it is expected that experimental efficiencies should drop off at high $u_{\rm min}$. While the predicted behavior of $u_{\rm min}$ is demonstrated by the figure, resolving this effect in practice would require many more events than currently observed.

## 5. CONCLUSION

While many prospects for learning more about ML events involve intensive follow-up observations aimed at resolving distortions to the standard ML light curve, few detailed calculations of rates and features of such distortions exist for realistic Galactic models. We have employed a detailed model to calculate the fraction of ML events that will exhibit a significant parallax distortion, as seen by the follow-up monitoring programs. We find that with frequent and precise observations of events in progress, from 10% up to 39% of all events arising from various lens-source pairings are expected to exhibit a parallax shift, including some events with $t_0 \lesssim 2$ months. Such events can be used to place an additional constraint among the parameters of interest (namely, $M_l$, $D_{\rm ol}$, and $v$) with reasonable precision, allowing one to express $M_l$ as a function of $D_{\rm ol}$ and thus better determine the characteristics of the lensing population. Failing to account for ML distortions, particularly blending, can lead

to errors in the inferred parameters (most notably $t_0$) that propagate into the inferred duration distribution and impact parameter distribution and that impact the assumed overall optical depth.

The most important application of analyzing such distortions is in discerning whether observed bulge events are due to structure in the bulge or excess mass in the form of substellar objects in the disk. However, the significance of such work extends to many areas. Determining the origin of the excess events will lead to a better understanding of Galactic structure and stellar populations, particularly the MF of low-mass stars in the disk and bulge. The latter relates directly to our understanding of the process of star formation. Moreover, if the bulge of our Galaxy is representative of relaxed stellar systems such as elliptical galaxies, then knowledge of the bulge luminosity function and dynamical structure will have implications for galaxy formation and evolution. Precise knowledge of the mass of the disk and bulge also constrains the halo mass and places strong limits on the dark matter content. If it can be determined that there is more mass in the bulge and/or disk, this implies less halo dark matter and has important consequences for the predicted event rates in direct and indirect searches for exotic dark matter (Jungman, Kamionkowski, & Griest 1996).

We wish to thank H. S. Zhao for providing us with data from his self-consistent model of the Galactic bar, and for helpful discussions. We also thank R. Olling for many insightful suggestions on constructing a reasonable model for the Galactic disk, as well as numerous helpful suggestions. We thank A. Gould, E. Wright, and R. M. Rich for very useful and detailed comments. This work was supported in part by the US Department of Energy under contract DE-FG02-92ER40699, and by NASA grant NAG 5-3091.

REFERENCES

Alard, C., et al. 1995, Messenger, 80, 31
Albrow, M., et al. 1996, preprint (astro-ph/9610128)
Alcock, C., et al. 1995a, ApJ, 445, 133
———. 1995b, ApJ, 454, L125
———. 1996a, ApJ, 461, 84
———. 1996b, ApJ, 463, L67
———. 1996c, ApJ, 471, 774
Aubourg, E., et al. 1993, Nature, 365, 623
Buchalter, A., Kamionkowski, M., & Rich, R. M. 1996, ApJ, 469, 676 (BKR)
Ciardullo, R., & Bond, H. E. 1996, AJ, 111, 2332
Crotts, A. P. S., & Tomaney, A. B. 1996, ApJ, 473, L87
Di Stefano, R., & Esin, A. A. 1995, ApJ, 448, L1
Gaudi, B. S., & Gould, A. 1996, preprint (astro-ph/9601030)
Gilliland, R., et al. 1993, AJ, 106, 2441
Gould, A., Bahcall, J. N., & Flynn, C. 1996, ApJ, 465, 759
Gould, A., Miralda-Escude, J., & Bahcall, J. N. 1994, ApJ, 423, L105
Griest, K., et al. 1991, ApJ, 372, L79
Han, C., & Gould, A. 1995, ApJ, 447, 53
Jungman, G., Kamionkowski, M., & Griest, K. 1996, Phys. Rep., 267, 195
Kamionkowski, M. 1995, ApJ, 442, L9
Kiraga, M., & Paczyński, B. 1994, ApJ, 430, L101 (KP)
Larson, R. 1986, MNRAS, 256, 641
Loeb, A., & Sasselov, D. 1995, ApJ, 449, L33
Maoz, D., & Gould, A. 1994, ApJ, 425, L67
Mihalas, D., & Binney, J. 1982, Galactic Astronomy (New York: Freeman)
Nemiroff, R. J., & Wickramasinghe, W. A. D. T. 1994, ApJ, 424, L21
Peale, S. J. 1996, Icarus, submitted (astro-ph/9612062)
Scalo, J. M. 1986, Fundamentals of Cosmic Physics (New York: Gordon & Breach)
Udalski, A., et al. 1994a, Acta Astron., 44, 165
Udalski, A., Szymanski, M., Kaluzny, J., Kubiak, M., Mateo, M., Krzeminski, W., & Paczyński, B. 1994b, Acta Astron., 44, 227
Witt, H. J., & Mao, S. 1994, ApJ, 430, 505
Zhao, H. S. 1996, MNRAS, 278, 488
Zhao, H. S., Rich, R. M., & Spergel, D. N. 1996, MNRAS, 282, 175
Zhao, H. S., Spergel, D. N., & Rich, R. M. 1995, ApJ, 440, L13